# A Simplified Dynamical System for Tropical Cyclone Intensity Prediction

Mark DeMaria*
NOAA/NESDIS, Fort Collins, CO 80523

Submitted to
Monthly Weather Review
January 2008

Corresponding Author:

Mark DeMaria
NOAA/NESDIS/StAR
1375 Campus Delivery
CIRA/CSU
Fort Collins, CO 80523
Mark.DeMaria@noaa.gov

**Abstract**

A simplified dynamical system for tropical cyclone intensity prediction based on a Logistic Growth Equation (LGE) is developed. The time tendency of the maximum sustained surface winds is proportional to the sum of two terms; a growth term and a term that limits the maximum wind to an upper bound. For storms over land the maximum wind is determined by an empirical inland wind decay formula. The model contains four free parameters, which are the growth rate, the maximum potential intensity (MPI), and two constants that determine how quickly the intensity relaxes towards the MPI. The MPI is estimated from an empirical formula as a function of sea surface temperature and storm translational speed. The adjoint of the LGE provides a method for finding the other three free parameters to make the predictions as close as possible to the National Hurricane Center best track intensities.

Results show that the LGE with parameters optimized for the full life cycle of individual storms can very accurately reproduce the intensity variations under the assumption that the growth rate is a linear function of the vertical shear estimated from global model analyses. A single set of free parameters is also found by fitting the model to more than 2400 Atlantic forecasts from 2001-2006. In this case, the growth rate is assumed to be a function of the vertical shear (S) and a convective instability parameter (C) determined from an entraining plume model. The soundings for the plume model are also from global model analyses in the storm environment. Results show that the LGE model solution (and some properties of real storms) can be explained by the evolution in the two-dimensional S-C phase space.

The application of the model to intensity forecasting is also described. Results from real time runs during the 2006 and 2007 hurricane seasons show that the LGE intensity errors were up to 17% smaller than those from the operational Statistical Hurricane Intensity Prediction Scheme (SHIPS).

## 1. Introduction

Tropical cyclone (TC) track forecast errors have decreased considerably over the past several decades. However, there have been only modest improvements in intensity forecasts (DeMaria et al, 2007). Because of the complexity of the physical processes affecting intensity changes, statistical forecast models have remained competitive with much more complex prediction systems. For this reason, the National Hurricane Center (NHC) continues to run a hierarchy of operational intensity models that range from the simple Statistical Hurricane Intensity Prediction Scheme (SHIPS) (DeMaria et al 2005) to the fully coupled atmosphere-ocean Hurricane Weather Research and Forecast (HWRF) system. The HWRF model became operational in 2007, and is the follow on to the National Centers for Environmental Prediction (NCEP) version of the Geophysical Fluid Dynamics Laboratory (GFDL) coupled hurricane model.

Several experimental intensity prediction systems of intermediate complexity have also been proposed. Emanuel et al (2004) showed that a three layer axisymmetric model coupled with a simplified ocean model can simulate many aspects of TC intensity changes when a parameterization for entrainment as a function of environmental vertical shear is included. Shen (2005) developed an intensity prediction system based on an energetics principal. In Shen's model, the prediction system is reduced to an ordinary differential equation for the integrated TC kinetic energy.

As opposed to physically based models described above, the operational SHIPS model is purely empirical. Multiple linear regression is used to relate factors from climatology, persistence, the atmosphere and ocean to intensity changes. The atmospheric variables are obtained from the NCEP global model and the oceanic variables are from

sea surface temperature (SST) analyses and satellite altimetry retrievals of ocean heat content. Predictors from GOES imagery are also included as measures of convective activity. An even simpler statistical model called SHIFOR is also run operationally at NHC. SHIFOR is also a linear regression model that only includes predictors from climatology and persistence (Knaff et al 2003). The SHIFOR forecasts are primarily used as a baseline for the evaluation of forecast skill. The experimental Florida State University Super- Ensemble (FSSE) is another example of an empirically based TC model. The superensemble methodology optimally combines the forecasts from a set of models (Krishnamurti et al 1999).

Over the past decade, SHIPS has generally been the most skillful of NHC's operational intensity forecast models, especially for the shorter range forecasts (DeMaria et al 2007). Although gradual improvements have been made to SHIPS by including predictors from new data sources such as GOES imagery and satellite altimetry, further improvements may be limited by the underlying linear nature of the model. Also, a relatively large number of predictors are needed to represent the intensity evolution. For example, the 2007 version of SHIPS included 21 predictors, and separate regression equations for each 6 hour forecast interval out to 120 h. In this study, a simple dynamical prediction system is introduced that can represent the basic evolution of TCs with a much smaller number of free parameters than SHIPS. Although the prediction system, which is based on a logistic growth equation (LGE), is still empirically based there is a closer relationship to physical processes through a direct inclusion of a maximum potential intensity (MPI) estimate. The complexity of this system lies between the energetics model of Shen (2005) and SHIPS.

The LGE is described in section 2, and the MPI estimation method is presented in section 3. Section 4 shows how the free parameters of the LGE can be estimated from the adjoint of the prediction model. Section 5 describes how the parameters fitted to a large number of storms can be used to define a two dimensional phase space (shear and instability) that helps to illustrate the roles of dynamic and thermodynamic factors on intensity changes. Real-time forecast results are presented in section 6.

## 2. The Logistic Growth Equation

The basic equation for the intensity prediction is based on an analogy with a differential equation commonly used to model population growth. For that application, the LGE can be written as

$$dP/dt = \kappa P - \mu P^2 \qquad (1)$$

where $P$ is the species population, $t$ is time and $\kappa$ and $\mu$ are constants. The first term on the right side represents reproduction, where the growth rate is proportional to the size of the existing population. The second is a mortality term that takes into account available resources and limits growth. This population model was first proposed by the Belgian mathematician Pierre F. Verhulst in 1838 (Murray 1979). Defining $K=\kappa/\mu$, then (1) becomes

$$dP/dt = \kappa P(K-P)/K \qquad (2)$$

For $P << K$, the population growth is exponential. However, as $P$ becomes large the growth rate slows down due to competition for resources. In the limit as $t \rightarrow \infty$ a steady state is reached where $P=K$. The quantity $K$ is called the carrying capacity and represents the maximum population that the environment can support.

For TC intensity prediction, the dependent variable in (1) is replaced by the maximum sustained surface wind V as a function of time. Viewing TC intensification from the point of view of a wind-induced surface heat exchange (WISHE) instability (Emanuel 1986), the surface energy flux depends on the current surface wind speed. Thus, the WISHE process is represented by the reproductive term in (1). The intensification process can not continue indefinitely and is limited to an upper bound (the MPI). This process is represented by the second term on the right in (2). The MPI concept was first proposed by Miller (1958), and theoretical formulas have been derived by Holland (1997) and Emanuel (1988). Empirical MPI formulas have also been developed from observations (e.g., DeMaria and Kaplan 1994; Whitney and Hobgood 1999). All of these MPI formulas depend on thermodynamic properties of the storm environment.

For the intensity prediction a generalized version of (1) is utilized where $\kappa$ and $\mu$ are time dependent and the power of two in the second term on the right is a arbitrary parameter greater than zero. With these assumptions, the intensity evolution is determined from

$$dV/dt = \kappa V - \beta V(V/V_{mpi})^n \qquad (3)$$

where $V_{mpi}$ is the MPI in terms of a maximum surface wind, $\kappa$ is the time dependent growth rate and $\beta$ and $n$ are positive constants. As will be described below, $\mu$ in (1) was replaced by $\beta/(V_{mpi})^n$ to make the steady state solution to (3) easier to interpret physically. Equation (3) has also been used in population growth studies (e.g., Thieme 2003). Similar to the SHIPS model it is assumed that the storm track is known. Then $V_{mpi}$ can be calculated from the SST and atmospheric soundings from model analyses or forecasts of

the storm environment. Similarly, $\kappa$ is assumed to be a function of environmental parameters such as vertical wind shear that can be calculated from analyses or model forecasts. Details of how the four parameters $V_{mpi}$, $\kappa$, $\beta$ and $n$ are estimated will be described in sections 3 and 4.

To better understand the behavior of (3), consider the case where the four parameters are all constants. For this case, the solution to (3) has two families of solutions. When $\kappa < 0$, both terms on the right side are always negative, so $V$ decays to zero. The solution also decays to zero when $\kappa=0$. When $\kappa>0$ the first term on the right dominates when $V$ is small, so $V$ increases exponentially. As $V$ increases, the second term becomes important, and in the limit as $t\rightarrow\infty$, a steady state solution is reached where $dV/dt$ is zero. Defining the steady state value of $V$ as $V_s$, setting $dV/dt = 0$ in (3) and solving for $V=V_s$ gives

$$V_s = (V_{mpi})(|\kappa|/\beta)^{1/n} \qquad (4)$$

The absolute value is included in (4) because $V_s$ can be used as a scale for $V$, whether $\kappa$ is positive or negative. Equation (4) shows that in the limit as $n\rightarrow\infty$, the steady state solution approaches $V_{mpi}$. As will be seen in section 4, when fit to observations the parameter $\kappa$ is nearly always less than $\beta$ and $n$ ranges from about 1 to 4. For these cases, the steady state solution is a fraction of $V_{mpi}$. $V_s$ can be interpreted as a modified MPI that takes into account additional storm environmental parameters such as vertical shear.

Even though (3) is nonlinear an analytic solution can still be determined. Assuming $\kappa\neq0$, equation (3) can be simplified by defining non-dimensional wind speed $U$ and time $\tau$ as

$$U = V/V_s \qquad (5)$$

$$\tau = |\kappa| t \tag{6}$$

Using (4)-(6), (3) can be written as

$$dU/d\tau = U(s - U^n) \tag{7}$$

where $s$ is the sign of $\kappa$ ($s=1$ if $\kappa>0$ or $s=-1$ if $\kappa<0$). The solution to (7) is given by

$$U(\tau) = U_o e^{s\tau}[1 + sU_o^n(e^{sn\tau}-1)]^{-1/n} \tag{8}$$

where $U_o$ is the initial value of $U$.

Figures 1 and 2 show $U(\tau)$ for several values of $U_o$ for $\kappa>0$ and $\kappa<0$. The solutions in Figs. 1 and 2 are for $n=3$. $U$ decays to zero with time for negative $\kappa$ and approaches 1 ($V=V_s$) for positive $\kappa$. The effect of the parameter n can be seen in Fig. 3, which shows $U(\tau)$ for positive $\kappa$ with $n=1,2 \ldots 5$. This parameter primarily affects the steepness of the $U$ curve. For the dimensional speed $V$, $n$ also affects the value of the steady state solution that is being approached as $t$ increases, as can be seen from (4).

The non-dimensional scaling in (5)-(6) is not valid for $\kappa=0$. For this case, the analytic solution of (3) is given by

$$V(t) = V_o[1 + \beta n t(V_o/V_{mpi})^n]^{-1/n} \tag{9}$$

where $V_o$ is the initial value of $V$. Equation (9) shows that the $V$ decays slowly to zero when $\kappa=0$.

Equation (3) is valid for the case where the storm center is over water. When the storm center is over land, the empirical inland wind decay model described by Kaplan and DeMaria (1995) is utilized. For that model, the maximum wind is reduced by a factor $R$ when the storm first moves over land to account for the difference in the surface roughness. If the storm moves back over the water, $V$ is divided by $R$. For the remaining time over land, the storm decays towards a background wind $V_b$ with an e-folding time

given by $\alpha$. Thus, the inland wind model is determined from the three specified parameters $R$, $V_b$ and $\alpha$. Kaplan and DeMaria (2001) developed a second set of parameters for higher latitude storms. For the dynamical system, the low-latitude parameters are used when the storm center is south of 36°N, the high-latitude parameters are used when it is north of 40°N, and linear interpolation is used between 36 and 40°N. $R=0.9$ at all latitudes, so only $\alpha$ and $V_b$ are linearly interpolated.

DeMaria et al (2006) showed that the inland wind model has a low bias for storms that move over islands and narrow land masses. They also showed that the bias can be corrected by multiplying $\alpha$ by the fraction of the storm area over land ($F$), where the storm area is defined as a circle with a radius of 111 km. With these assumptions, the evolution of $V$ when the storm is over land is determined from

$$dV/dt = -\alpha(V-V_b) \qquad (10)$$

where $\alpha$ includes the fractional area correction $F$. Because of the factor $F$ and the linear interpolation as a function of latitude, both $\alpha$ and $V_b$ are specified functions of time. Equations (3) and (10) will be referred to as the Logistic Growth Equation Model (LGEM).

**3. Maximum Potential Intensity estimation**

As described in Section 2, several theoretical and empirical methods have been proposed to estimate the MPI. The two formulations considered here are the empirical formula for the Atlantic basin developed by DeMaria and Kaplan (1994) (refereed to as DK) and the theoretical estimate from Bister and Emanuel (1998) (refereed to as BE). The DK formula depends only on the SST, which is estimated from the weekly Reynold's SST analyses at the storm center. The BE formula requires an SST and a

temperature and moisture sounding. The SST for the BE estimate is also from the Reynold's analyses and the soundings are determined by averaging the NCEP global forecast system (GFS) model analysis in an annulus from 200 to 800 km from the storm center.

Figure 4 shows a scatter plot of the DK and BE MPI estimates for 1982-2006. These cases are from the Atlantic SHIPS model developmental sample, which includes all named storms, as well as depressions that never reached tropical storm strength. The extratropical stage is not included. This figure shows that the two MPI estimates are highly correlated (the correlation coefficient is 0.89). However, in some cases the BE MPI estimates are zero. These are mostly high latitude cases where the storm may have had an energy source from baroclinic processes not included in the BE theory or for storms that moved quickly over cold water and did not have time reach equilibrium with the thermodynamic environment. In equation (3), an MPI of zero would be problematic due to the $V_{mpi}$ factor in the denominator. For this reason, the DK formula was used to estimate $V_{mpi.}$

The DK formula was developed in a storm relative coordination system, so a fraction of the storm translational speed is added to the DK MPI estimate from the equation developed by Schwerdt et al (1979). The MPI is increased by $1.5c^{0.63}$ where $c$ is the translational speed in knots.

**4. Parameter estimation**

Once $V_{mpi}$ is determined, the remaining parameters in (3) that need to be specified are $\kappa$ as a function of time and the constants $\beta$ and $n$. It will be assumed that $\kappa$ is a linear function of large scale variables such as vertical shear, which are known functions of

time. For the parameter estimation derivation the case where $\kappa$ is a linear function of just one variable $x(t)$ is considered, but the results can easily be generalized to multiple variables. With this assumption, $\kappa$ is given by

$$\kappa(t) = ax(t) + b \tag{11}$$

and the parameter estimation problem is reduced to the determination of the 4 constants $\beta$, $n$, $a$ and $b$.

A method for estimating model parameters has been developed as part of data assimilation systems. For example, Zhu and Navon (1999) showed that the adjoint of a global forecast model can be used to optimize diffusion and boundary layer flux parameters. A similar method is applied to LGEM. In the general case with variable coefficients, (3) must be solved numerically. The numerical solution is described first, and then the adjoint of the discretized system and the application to parameter estimation is presented.

Whether over water or land, LGEM contains exponentially growing or decaying solutions. Therefore, a forward time differencing scheme can be used. Letting $t$ be discretized using

$$t_m = m\Delta t,\ m=0,\ 1,\ 2\ \ldots\ M \tag{12}$$

and any variable with a subscript m be evaluated at $t_m$ ,then the finite difference form of the combined equations (3) and (10) can be written as

$$V_{m+1} = R_m V_m + \{\delta_m[\kappa_m R_m V_m - \beta(R_m V_m / V_{mpim})^n R_m V_m] - \varepsilon_m[\alpha_m(R_m V_m - V_{bm})]\}\Delta t \tag{13}$$

In (13), $\delta_m = 1$ if the storm center is over water at time $t_m$ and $\delta_m = 0$ if the storm is over land, and vice versa for $\varepsilon_m$. The $R_m$ factor takes into account the reduction in wind speed when the storm first moves from water to land and the increase when it moves back over

the water, which is part of the inland wind model. Mathematically, $R_m=R$ for the first time step over land, $R_m=1/R$ for the first time step over water and $R_m=1$ for all other time steps. Given the initial condition $V=V_o$, (13) can be used to find $V_m$ for $m=1,2 \ldots M$. The time scale of the growth or decay of $V$ is on the order of 12 h, so a one hour time was found to be adequate for stability and accuracy. Equation (13) will be referred to as the forward model.

The model parameters will be chosen so that the solution of the forward model is as close to observed intensity values as possible. The observations are the maximum sustained surface winds from the NHC best track, which are available at 6 hour intervals. The best track intensity estimates were linearly interpolated to the one hour time step of the forward model and are denoted by $O_m$. Because the best track intensities are reported in knots rounded to the nearest 5, units of knots are used for $V_m$ and $O_m$. For a model integration of length $t_M$, the model error $E$ is defined as

$$E = 1/2 \sum_{m=1}^{M} (V_m - O_m)^2 \tag{14}$$

If the gradient of $E$ with respect to the parameters $\beta$, $n$, $a$ and $b$ could be determined, the optimal values could be found using a gradient descent algorithm. This is accomplished using the method of Lagrange multipliers where the forward model equations are appended to $E$ as constraints. Letting (13) be represented symbolically by

$$V_m = R_{m-1} V_{m-1} + G_{m-1} \Delta t \tag{15}$$

then the Lagrange function $J$ can be written as

$$J = E + \sum_{m=1}^{M} \lambda_m [V_m - (R_{m-1} V_{m-1} + G_{m-1} \Delta t)] \tag{16}$$

where $\lambda_m$ are Lagrange multipliers. Setting the derivative of $J$ with respect to $V_m$ to zero gives the adjoint model

$$\lambda_M = -(V_m - O_m) \tag{17}$$

$$\lambda_m = \lambda_{m+1}\{R_m + \delta_m \Delta t R_m [\kappa_m - \beta(n+1)( R_m V_m / V_{mpi\,m})^n] - \varepsilon_m \alpha_m R_m \Delta t\} - (V_m - O_m) \tag{18}$$

Note that the adjoint equation (18) is integrated backwards in time to give $\lambda_m$ for $m=M-1$, $M-2, \ldots, 1$ after being initialized with (17).

Using the discretized version of (11), the gradients of $J$ with respect to the parameters $\beta$, $n$, $a$ and $b$ are given by

$$\partial J/\partial \beta = \sum_{m=1}^{M} \lambda_m \delta_{m-1} \Delta t (R_{m-1} V_{m-1} / V_{mpi\,m-1})^n R_{m-1} V_{m-1} \tag{19}$$

$$\partial J/\partial n = \sum_{m=1}^{M} \lambda_m \delta_{m-1} \Delta t \beta (R_{m-1} V_{m-1} / V_{mpi\,m-1})^n \ln(R_{m-1} V_{m-1} / V_{mpi\,m-1})\, R_{m-1} V_{m-1} \tag{20}$$

$$\partial J/\partial a = -\sum_{m=1}^{M} \lambda_m \delta_{m-1} \Delta t R_{m-1} (x_{m-1} V_{m-1}) \tag{21}$$

$$\partial J/\partial b = -\sum_{m=1}^{M} \lambda_m \delta_{m-1} \Delta t R_{m-1} (V_{m-1}) \tag{22}$$

and are used to find the four constants that minimize the error in the forward model as part of a steepest descent algorithm. In each iteration, the forward model is integrated to give $V_m$, the adjoint model is integrated to give $\lambda_m$, the gradients are calculated and then the four constants are adjusted in the direction opposite to the sign of the gradient, with an adjustment that is proportional to the magnitude of the gradient. The components of the gradient are scaled to account for the differing units of the four constants. If $\kappa$ in (11) is a linear function of additional variables, the gradient will contain additional components of the form of (21).

As a first test of the parameter estimation, the four constants that minimize the error of the forecast of the entire life time of a single storm were determined. The test case is Hurricane Frances (2004), which formed west of the Cape Verde Islands on 25 Aug at 0000 UTC, intensified to a category four hurricane over the mid-Atlantic, and weakened to a category two storm before striking southeast Florida north of Palm Beach (Beven 2004). Frances weakened to a tropical storm as it crossed Florida, briefly re-entered the Gulf of Mexico, but did not regain hurricane intensity. Frances made a second landfall in the Big Bend region of northwest Florida and transitioned to an extratropical cyclone over West Virgina. LGEM was initialized on 25 Aug at 0000 UTC with an intensity of 25 kt and was run until 8 Sept at 1800 UTC (14.75 days), which was just before the extratropical transition. The MPI along the observed track was estimated using the empirical formula described in section 3 and the vertical shear was determined from the GFS analyses using the same basic method as for the 2007 SHIPS model. The vertical shear is the magnitude of the 850 to 200 hPa vector wind difference, where the winds at 850 and 200 hPa are averaged over a circular area centered on the storm with a radius of 500 km. The SHIPS model was modified in 2007 to use a smaller area than in the version described by DeMaria et al (2005). The variable $x_m$ in (21) is the vertical shear normalized by subtracting the sample mean and dividing by its standard deviation.

The steepest descent algorithm converged after about 100 iterations and the mean absolute error (MAE) of the intensity prediction over the 14.75 day forecast period was reduced to a surprisingly low 4.2 kt. Figure 5 shows the maximum wind from the LGEM prediction, the NHC best track and the MPI. This figure shows that the fitted LGEM reproduces nearly every aspect of the intensity variation of Frances. The largest error

occurs near 280 h where the inland wind model predicted too much decay as the storm crossed Florida. However, the difference between the LGEM prediction and the best track is less than about 10 kt for the rest of the integration.

The GFS fields for the vertical shear calculation were obtained from the SHIPS model data archive. The SHIPS model uses operational analyses for the dependent sample beginning in 2001 and reanalysis fields before 2001. Additional tests of the parameter estimation were performed for long-lived storms from 2001 to 2006. Two storms were chosen from each year, except for 2005, where three storms were used. The 13 cases are listed in Table 1 and were selected to include storms over different parts of the Atlantic basin and different times during the hurricane season. Table 1 also shows the values of the parameters that minimize the LGEM prediction for each storm and the MAE after convergence of the steepest descent algorithm. This Table shows that the MAE was reduced to between 4.2 and 10.6 kt for all 13 storms, which indicates that the LGEM can reproduce many aspects of the observed intensity changes from the SST and vertical shear with just four free parameters.

Table 1 shows the values of the four parameters for each storm case, and the 13 storm average. Although there is considerable variability in the coefficients, there is also some consistency. The parameter $a$ values are all negative except for Hurricane Katrina. As can be seen from (11), when $a$ is negative, the growth rate decreases as the shear increases. For Katrina, the shear was low for nearly the entire storm lifetime, so there was little information on the relationship between the intensity changes and shear. In every case except Hurricane Epsilon, $\beta$ is larger than $b$. Since $b$ is the mean value of $\kappa$ the steady state solution $V_s$ defined by (4) to which the intensity is being relaxed is, on

average, a fraction of the MPI. The modification of $V_{mpi}$ by the vertical shear and other synoptic factors is described in greater detail in the next section when a single set of parameters is fit to LGEM forecasts for a large sample of storms.

In many cases the deviation of the fitted LGEM forecast from the NHC best track can be related to storm characteristics not included in the model. As an example of this, Fig. 6 shows the fitted LGEM prediction and best track for Hurricane Katrina. The LGEM prediction is generally too high from about 84 to 96 hr. The observed intensity stayed fairly constant during this period while the storm went through an eyewall replacement cycle (Knabb et al 2005). The intensity changes during this period were determined by inner core processes, rather than large scale processes. From about 100 to 120 h, Katrina rapidly intensified to 150 kt and the LGEM prediction underestimated the maximum wind. The storm moved over a warm ocean eddy during this period (Mainelli et al 2008), which was not represented in the model since the SST was fairly constant during this time. It might be possible to include the effect of warm eddies by developing a more general MPI formula that includes sub-surface ocean information.

**5. Generalized Model Fitting**

The results in section 4 show that the mathematical framework of the LGEM can accurately reproduce most of the intensity variations when fitted to individual TCs. Unfortunately, the parameters in Table 1 show considerable storm to storm variation. If this system was used for real time prediction, a general set of parameters would need to be determined. For this purpose, the model was simultaneously fitted to all of the storm cases from 2001-2006. To better represent how the model would be used for prediction, each storm case was divided into a sequence of 5 day forecasts. For example, if a

particular storm lasted for 6 days (144 h), it would be divided into 24 forecasts from 0 to 120 h, 6 to 126 h, … 138 to 144 h. The first 5 cases would be 120 h predictions, the next would be 114 h and the last would be 6 h. The 2001-2006 sample includes 2465 forecast cases at 6 h, decreasing to 836 cases at 120 h.

The 2007 version of the Atlantic SHIPS model included 21 predictors based on climatology, persistence, atmospheric and oceanic factors. The majority of the atmospheric and oceanic predictors are related to either the dynamics of the storm environment (e.g., vertical shear and upper level divergence) or the thermodynamics of the storm environment (e.g., relative humidity, upper-level temperature). In the parameter estimation procedure, the only thermodynamic information included is the SST used in the calculation of the MPI. To better account for thermodynamic effects of the storm environment, a second predictor $C$ was included in the estimation of $\kappa$. This predictor was designed to measure the convective instability of the storm environment.

As summarized by Zipser (2003), instability indices such as Convective Available Potential Energy (CAPE) or Lifted Index (LI) that have been used in the mid-latitudes are not appropriate for the tropics because some of the neglected factors such as the weight of the condensate and entrainment are of first-order importance. For this reason, the $C$ predictor was determined from an entraining plume model.

The plume model uses temperature and moisture soundings from the GFS analyses averaged over an annulus from 200 to 800 km from the storm center and the Reynold's SST for the surface temperature. The plume is initialized with a surface-based parcel with an upward vertical velocity of 8 $ms^{-1}$. This fairly large value was chosen so that the parcel would reach its lifting condensation level for most soundings. The

evolution of the parcel is determined by the thermodynamic formulation of Ooyama (1990), where the ice phase is included by considering a single moisture variable that behaves like water for temperatures above $0^oC$ and like ice below $0^oC$. Entrainment is included by assuming that the mass entrainment rate is inversely proportional to the radius of the parcel (Simpson and Wiggert 1969), so that

$$(1/M)dM/dz = C_E/r \quad (23)$$

where $M$ is the parcel mass, $z$ is height, $r$ is the parcel radius and $C_E$ is the entrainment rate (specified to be 0.1). The initial parcel radius is 0.5 km, which is a reasonable value for tropical convection (LeMone and Zipser 1980). The calculation includes the weight of the condensate and virtual temperature effects on the buoyancy. Precipitation was included by assuming that the rate of fallout of the condensate from the parcel is proportional to the amount of condensate present, with a proportionality constant of $600^{-1}$ $s^{-1}$. The predictor $C$ is the 0 to 15 km average of the vertical velocity of the parcel in the plume model.

Figure 7 shows vertical velocity profiles from the plume model for a mean Atlantic tropical sounding (Dunion 2008). The sounding is a composite from Caribbean stations that were determined to be uninfluenced by the stable Saharan Air Layer (SAL). The effects of condensate weight and entrainment can be seen by comparing the three profiles in Fig. 7. Without these two effects, the vertical velocities are unrealistically large, and the $C$ predictor would have little utility in diagnosing the convective instability. With both effects included, the vertical velocities are on the high side but within the range of what has been observed in tropical convection (Zipser 2003).

With the additional predictor $C$, the growth rate is given by

$$\kappa = b + a_1 S + a_2 C + a_3 SC \qquad (24)$$

where $S$ is the 850-200 hPa vertical shear. Both $S$ and $C$ are normalized by subtracting the sample mean and dividing by the standard deviation. For the 2001-2006 sample, the mean and standard deviation are 9.0 and 5.6 $ms^{-1}$ for S and 7.5 and 4.1 $ms^{-1}$ for C. When $S$ and $C$ are normalized in this way, the constant $b$ in (24) is the mean value of $\kappa$. The $a_3$ term is included in (24) to allow for nonlinear interactions between the vertical shear and instability.

The adjoint model was used to find the six constants $\beta$, $n$, $a_1$, $a_2$, $a_3$ and $b$ that minimize the forward model error for the 2465 forecasts from 2001-2006. To determine the impact of the $S$ and $C$ terms in (24), the minimization was also performed with just $b$, just $b$ and $a_1$, just $b$ and $a_2$, and just the $b$, $a_1$ and $a_2$ terms. Figure 8 shows the MAE of the intensity forecasts versus time for four of the five combinations of terms in (24) (the $b$, $a_1$ and $a_2$ case was omitted for clarity of the diagram). Relative to the case with just a mean value of $\kappa$ (just the $b$ term), the biggest reduction in model error comes from adding the $S$ term. The $C$ term also provides some reduction in the error, with the best result with all four terms included. The MAEs in Fig. 8 are much larger than those for the model fits to the individual storms shown in Table 1. That is not surprising since several thousand forecasts are being fit with just six free parameters. However, the MAE values in Fig. 8 are comparable to those from fitting the intensity changes in the SHIPS model, which includes 420 regression coefficients (21 predictors at 20 forecast times).

Table 2 shows the values of the constants determined by the optimization procedure for the four combinations of predictors in (24). The best fit occurs when all four terms are included in estimation of $\kappa$. Using four-term values for $\beta$ and $n$ and the

value of $b$ for the average value of $\kappa$, the steady solution defined by (4) is only about 58% of the MPI. This result is consistent DeMaria and Kaplan (1994) and Emanuel (2000) who showed that TCs rarely reach their MPI.

The roles of dynamic and thermodynamic factors on the LGEM intensity changes can be seen by considering $\kappa$ as a function of $S$ and $C$. As described in section 2, $\kappa$ determines the rate of growth towards the steady state solution when positive, or the rate of decay towards zero when negative. Figure 9 shows contours of $\kappa$, where $S$ and $C$ range from zero to the mean plus three standard deviations. For $S$ less than about 12 $ms^{-1}$, $\kappa$ increases with $C$ and decreases with $S$. Over most of this region the influence of $S$ is more important than $C$ since the contours are almost vertical. For low values of $C$, the influence of $S$ decreases. Physically, this result suggests that as long as there is some potential for convection, the primary influence on TC intensification is the vertical shear. For larger values of shear, $\kappa$ becomes negative, indicating dissipation. Also for large values of shear, the relationship between $C$ and $\kappa$ is reversed. This is probably due to the influence of higher latitude storms that are beginning to take on extra-tropical characteristics. For these storms, the $C$ values tend to be low, but the $S$ values are high. The growth rate is less negative or slightly positive for these types of storms.

Equation (4) can be written as

$$V_s / V_{mpi} = (|\kappa|/\beta)^{1/n} \qquad (25)$$

Using the fitting parameters from Table 2, (25) and (24) can be used to calculate the ratio of the steady state solution to the SST-based MPI estimate as a function of $S$ and $C$. This ratio can be interpreted as an MPI adjustment factor (MAF) that takes into account shear and convective instability. Figure 10 shows that for very low $S$ and high $C$, the MAF is

close to one. There is a small region in the upper left side of the diagram where the MAF is a little larger than one. As expected, the MAF decreases to zero as the shear becomes large, and there is greater sensitivity to *S* than *C*. The effect of shear on the MPI in Fig. 10 is qualitatively similar to that described by Zeng et al (2008). The reversal of the effect of *C* on MAF for large values of *S* is again probably due to storms beginning extra-tropical transition.

Figures 9 and 10 show that the location in the *S*-*C* plane determines the storm intensity evolution in the LGEM. Thus, it is instructive to consider the *S*-*C* trajectory of storms as they evolve. Figure 11 shows the *S*-*C* evolution for Hurricane Katrina from its initial formation on 23 August until just before its Gulf Coast landfall on 29 August. The storm spent nearly its entire lifetime in the upper left quadrant of the diagram, which indicates that the shear was below average and the convective potential was above average. Katrina underwent at least one eyewall replacement cycle and also rapidly intensified.

Figure 11 also shows the average *S* and *C* values for the 108 cases that rapidly intensified (RI), the 31 cases that had secondary eyewall formation (SEF), and the 20 cases that were identified as annular hurricanes (AH). Rapid intensification cases are those where the maximum winds increased by 30 kt or more in the following 24 h (Kaplan and DeMaria 2003), the SEF cases were identified from microwave imagery (J. Kossin and Sitkowski 2008), and the annular hurricanes are fairly steady state storms with large eyes and few rainbands as determined by Knaff et al (2008). The RI and SEF points are located in the upper left quadrant, similar to Katrina. However, the AH point is in the lower left quadrant. This result indicates that low vertical shear is important for all

three types of storms, but the convective instability helps to distinguish between RI/SEF behavior and AH behavior.

Figure 12 shows the *S*-*C* evolution for Hurricane Claudette (2003) from its formation on 08 July to just before its landfall in Texas on 15 July. This storm transformed from a wave into a tropical storm in the Central Caribbean and briefly became a category 1 hurricane after about 2 days before weakening to a tropical storm due to interaction with fairly strong vertical shear (Beven 2003). The storm moved into the Gulf of Mexico and remained a tropical storm until just before its landfall along the central Texas coast when it again strengthened to a category 1 hurricane. The storm was in the upper right quadrant of the *S*-*C* diagram for most of its lifetime with *S* values near 12 $ms^{-1}$ and *C* values near 10 $ms^{-1}$. In this quadrant the favorable convective instability is balanced by unfavorable shear. Fig. 9 shows that for these values of *S* and *C*, $\kappa$ is small but positive. Infrared satellite imagery for Claudette (not shown) indicated that Claudette maintained deep convection, but it was asymmetric and highly transient. This result suggests that storms in this part of the phase space have a very unsteady behavior and do not intensity very rapidly. Just before landfall Claudette moved into the upper left quadrant of the *S*-*C* phase space, which is consistent with its re-intensification to a hurricane.

The above results suggest that monitoring the *S*-*C* evolution might be useful for anticipating TC behavior. Figure 13 shows a conceptual diagram further illustrating this idea. The various behaviors would not be represented by single points in a diagram like Fig. 13, but, probability distributions in the S-C plane could be determined from large

samples of various types of storms. The locations of the maximum probabilities could also be determined as were shown for the RI, SEF and AH cases in Fig. 11.

**6. Forecast Applications**

The LGEM requires the SST, land indicator and vertical soundings of wind, temperature and moisture along the storm track. In the results presented so far, these were obtained along the best track from Reynold's SST and GFS model analyses. If the observed track were replaced by a forecast track and the GFS analyses were replaced by GFS forecast fields, this system could be used for operational intensity prediction.

A version of LGEM with a different fitting technique for $\kappa$ was run in real time during 2006 and 2007 seasons for all storms in the Atlantic and east Pacific, as part of the processing for the operational SHIPS model. For these tests, the adjoint fitting technique was not developed yet. Instead, (3) was solved for $\kappa$ to give

$$\kappa = (1/V)dV/dt + \beta(V/V_{mpi})^n \qquad (26)$$

$V_{mpi}$ was calculated using the method described in section (3) and $dV/dt$ was determined from the best track intensities using a 24 h centered time difference. Initial guesses were made for the parameters $\beta$ and $n$, and the best tracks were divided into a sequence of 5 day forecasts in the same way as in section 5. With these assumptions, (26) was used to calculate "observed" values of $\kappa$ for each of the 5-day forecasts. Then, regression equations were developed for the estimation of $\kappa$ using the same predictors as in the SHIPS model, but without those from satellite data or the quadratic terms (see DeMaria et al, 2005). This procedure was repeated with several values of $\beta$ and $n$ and those that maximized the variance explained in the linear prediction of $\kappa$ were determined. The final values of $\beta$ and $n$ were 1/24 $h^{-1}$ and 2.5, respectively. Persistence was included in the

regression by calculating $\kappa$ at the beginning of each forecast from the intensity values from the previous 12 h (a one-sided difference was used for *dV/dt* in this case), which was used as a predictor for $\kappa$ at each forecast time. A separate set of regression equations was used to predict $\kappa$ from 0 to 120 h.

The real time runs used the same input as the operational SHIPS model, including the NHC operational forecast track and predictors estimated from GFS forecast fields. Figure 14 shows the percent improvement of the average intensity errors of the LGEM forecasts relative to the SHIPS forecasts for the combined 2006 and 2007 real time sample. The LGEM forecast errors were larger than those of SHIPS at the early forecast periods, but were up to 17% smaller at the longer times in the east Pacific. In the Atlantic, the LGEM errors were up to 10% smaller than those of SHIPS. These results indicate that the formalism of the LGE provides improvement relative to the linear regression used in the SHIPS model, since both forecasts used the same input data.

The real time versions of LGEM that were run in 2006 and 2007 had some simplifications relative to the version described in section 5. The developmental sample for the regression equations for $\kappa$ was restricted to cases where the storm was over the water during the 24 h period used to evaluate *dV/dt*. This restriction is not necessary with the adjoint minimization procedure. Also, the error in $\kappa$ was minimized, rather than the intensity errors as in the adjoint version. In addition, the real time version used separate regression equations at each forecast interval, rather than a constant set of parameters, and did not make use of the entraining plume model. For the 2008 season, a more general version of LGEM will be tested. As shown in section 4, the fit of the LGEM provided very accurate MAEs for individual storms. This result suggests that it might be possible

to fit the past history of a given storm up to the forecast interval to adjust some of the constants in (24) relative to their values determined from the large sample. This would provide an alternate method for including persistence information in the LGEM prediction.

**7.0 Concluding Remarks**

A simplified dynamical system for TC intensity prediction based on a Logistic Growth Equation (LGE) was developed. The application of the LGE was based on an analogy with population dynamics, and constrains the solution to lie between zero and an upper bound intensity. When the storm track is over land, the maximum wind is determined by an empirical inland wind decay formula. The LGE model (LGEM) contains four free parameters, which are the growth rate, the MPI, and two constants that determine how quickly the intensity relaxes towards the MPI. The MPI was estimated from an empirical formula as a function of SST and storm translational speed. The adjoint of the LGEM provides a method for finding the other three free parameters to make the predictions as close as possible to the NHC best track intensities.

Results showed that the LGEM with parameters optimized for the full life cycle of individual storms can very accurately reproduce the intensity variations under the assumption that the growth rate is a linear function of the vertical shear estimated from global model analyses. A single set of free parameters was also found by fitting the model to all Atlantic forecasts from 2001-2006. In this case, the growth rate is assumed to be a function of the vertical shear ($S$) and a convective instability parameter ($C$) determined from an entraining plume model that used soundings from global model. It

was shown that the LGEM solution (and some properties of real storms) can be explained by the evolution in the two-dimensional *S*-*C* phase space.

The application of the LGEM to real time forecasting was also described. Results from real time runs during the 2006 and 2007 hurricane seasons show that the LGEM intensity errors were up to 17% smaller than those from the operational SHIPS model.

The deviations from the LGEM fit to individual storms could often be explained by physical processes not included in this simple system, such as eyewall cycles or movement over warm ocean eddies. The LGEM might be further improved by developing a modified MPI estimate that includes sub-surface ocean information. It might also be possible to use satellite imagery to identify storms undergoing eyewall cycles and to develop a modification to the growth rate parameter. Also, for short term forecasts, high resolution temperature and moisture soundings from satellite retrievals might be used in the storm environment as input to the convective instability parameter, or in a more general MPI formulation that included the atmospheric thermodynamic information in addition to the SST. Also, the real time version of the LGEM run at NHC in 2006 and 2007 did not use the adjoint model to determine the model parameters or to assimilate the past history of each storm up to the time of the forecast. These are topics for future research.

## Acknowledgments

The author thanks Kerry Emanuel for providing his MPI code, Jason Dunion for the mean tropical sounding and Jim Kossin and Matt Sitkowski for their secondary eyewall formation database. The views, opinions, and findings in this report are those of the author and should not be construed as an official NOAA or U. S. government position, policy, or decision.

## REFERENCES


Beven, J.L., 2003: Tropical Cyclone Report, Hurrican Claudette, 8-17 July 2003. Available from http://www.nhc.noaa.gov/2003claudette.shtml .

_____, 2004: Tropical Cyclone Report, Hurricane Frances, 25 August-8 September 2004. Available from http://www.nhc.noaa.gov/2004frances.shtml .

Bister, M., and K.A. Emanuel, 1998: Dissipative heating and hurricane intensity. *Meteor. Atmos. Phys*., **50**, 233-240.

DeMaria, M. and J. Kaplan, 1994: Sea surface temperature and the maximum intensity of Atlantic tropical cyclones. *J. Climate*, **7**, 1324-1334.

_____, J.A. Knaff, and C.R. Sampson, 2007: Evaluation of Long-Term Trends in Operational Tropical Cyclone Intensity Forecasts. *Meteor. and Atmos. Phys.*, **59**, 19-28.

_____, _____, and J. Kaplan, 2006: On the decay of tropical cyclone winds crossing narrow landmasses, *J. Appl. Meteor*., **45**, 491-499.

_____, M. Mainelli, L.K. Shay, J.A. Knaff and J. Kaplan, 2005: Further Improvements in the Statistical Hurricane Intensity Prediction Scheme (SHIPS). *Wea. Forecasting*, **20**, 531-543.

Dunion, J., 2008, personal communication.

Emanuel, K.A., 1986: An air-sea interaction theory for tropical cyclones. Part I: Steady-state maintenance. *J. Atmos. Sci*., **43**, 585-605.

_____, 1988: The maximum intensity of hurricanes. *J. Atmos. Sci*., **45**, 1143-1155.

_____, 2000: A statistical analysis of tropical cyclone intensity. *Mon. Wea. Rev.*, **128**, 1139-1152.

_____, C. DesAutels, C. Holloway and R. Korty, 2004: Environmental controls on tropical cyclone intensity. *J. Atmos. Sci.*, **61**, 843-858.

Holland, G.J., 1997: The maximum potential intensity of tropical cyclones. *J. Atmos. Sci.*, **54**, 2519-2541.

Kaplan, J., and M. DeMaria, 1995: A simple empirical model for predicting the decay of tropical cyclone winds after landfall. *J. Appl. Meteor.*, **34**, 2499-2512.

_____, and _____, 2001: On the decay of tropical cyclone winds after landfall in the New England area. *J. Appl. Meteor*., **40**, 280-286.

_____, and _____, 2003: Large-scale characteristics of rapidly intensifying tropical cyclones in the North Atlantic basin. *Wea. Forecasting*, **18**, 1093-1108.

Knabb, R.D., J.R. Rhome and D.P. Brown, 2005: Tropical Cyclone Report, Hurricane Katrina, 23-30 August 2005.

Available from http://www.nhc.noaa.gov/pdf/TCR-AL122005_Katrina.pdf .

Knaff, J.A., T.A. Cram, A.B. Schumacher, J.P. Kossin and M. DeMaria, 2008: Objective identification of annular hurricanes. *Wea. Forecasting*, **23**, in press.

_____, M. DeMaria, B. Sampson, and J.M. Gross, 2003: Statistical, Five-Day Tropical Cyclone Intensity Forecasts Derived from Climatology and Persistence. *Wea. Forecasting*, **18**, 80-92.

Kossin, J. and M. Sitkowski, 2008, personal communication.

Krishnamurti, T.N., C.M. Kishtawal, T. LaRow, D. Bachiochi, Z. Zhang, C.E. Williford, S. Gadgil, and S. Surendran, 1999: Improved skills for weather and seasonal climate forecasts from multimodel superensemble. *Science,* **285**, 1548-1550.

LeMone and Zipser, 1980: Cumulonimbus vertical velocity events in GATE. Part I: Diameter, intensity and mass flux. J. Atmos. Sci., **37**, 2444-2457.

Mainelli, M., M. DeMaria, L.K. Shay and G. Goni, 2007: Application of oceanic heat content estimation to operational forecasting of recent Atlantic category 5 hurricanes. *Wea. Forecasting*, **23**, in press.

Miller, B.I., 1958: On the maximum intensity of hurricanes. *J. Meteor*., **15,** 184-195.

Murray, B.G., 1979: Physiological Ecology. Academic Press, Inc., 111 Fifth Ave., NY, NY, 10003. ISBN 0-12-511750-4, 212 p.

Ooyama, K.V., 1990: A thermodynamic foundation for modeling the moist atmosphere. *J. Atmos. Sci*., **47**, 2580-2593.

Schwerdt, R.W., F.P. Ho, and R.R. Watkins, 1979: Meteorological criteria for standard project hurricane and probable maximum hurricane windfields, Gulf and East Coast of the United States, NOAA Tech. Rep. NWS 23, 317 pp. [Available from NWS NOAA, U.S. Department of Commerce, 8060 13th St. Silver Spring, MD 20910.]

Shen, W., 2005: A simple prediction model of hurricane intensity. *Quar. J. Roy. Meteor. Soc.*, **131**, 2887-2906.

Simpson, J., and V. Wiggert, 1969: Models of precipitating cumulus towers. *Mon. Wea. Rev*., **97**, 471-489.

Thieme, H.R., 2003: Mathematics in Population Biology. Princeton University Press, 41 William St., Princeton, NJ, 08540. ISBN 0691-09290-7, 543 p.

Whitney, L.D., and J. S. Hobgood, 1997: The relationship between sea surface temperature and maximum intensities of tropical cyclones in the eastern North Pacific Ocean. *J. Climate*, **10**, 2921-2930.

Zeng, Z., L. Chen and Y. Wang, 2008: An observational study of environmental dynamical control of tropical cyclone intensity in the Atlantic. *Mon. Wea. Rev*., **136**, in press.

Zhu, Y., and I.M. Navon, 1999: Impact of parameter estimation on the performance of the FSU global spectral model using its full-physics adjoint. *Mon. Wea. Rev.*, **127**, 1497-1517.

Zipser, E., 2003: 5: Some views on "Hot Towers" after 50 years of tropical field programs and two years of TRMM data. *Cloud Systems, Hurricanes, and the Tropical Rainfall Measuring Mission (TRMM – A Tribute to Dr. Joanne Simpson.* Meteorological Monographs, Amer. Meteor. Soc., **29**, 49-57

Table 1. Values of the LGE model parameters for 13 Atlantic storms from the 2001-2006 seasons and the mean absolute error of the intensity prediction. The starting data/time, LGE model integration length and peak intensity of the each storm from the NHC best track are also shown.

| Name | Year | Start | Length (day) | Peak Intensity (kt) | n | β ($hr^{-1}$) | b ($hr^{-1}$) | a ($hr^{-1}$) | MAE (kt) |
|---|---|---|---|---|---|---|---|---|---|
| Felix | 2001 | 10 Sep 06 UTC | 8.75 | 100 | 3.9 | 0.0478 | 0.0058 | -0.0117 | 9.4 |
| Olga | 2001 | 24 Nov 00 UTC | 10.75 | 80 | 4.3 | 0.1288 | 0.0095 | -0.0196 | 6.3 |
| Isidore | 2002 | 17 Sep 12 UTC | 10.00 | 110 | 3.4 | 0.0276 | 0.0145 | -0.0001 | 5.2 |
| Kyle | 2002 | 20 Sep 18 UTC | 21.75 | 75 | 2.1 | 0.0559 | 0.0050 | -0.0102 | 7.6 |
| Claudette | 2003 | 08 Jul 18 UTC | 8.25 | 75 | 2.5 | 0.0492 | 0.0099 | -0.0056 | 5.4 |
| Isabel | 2003 | 06 Sep 00 UTC | 13.25 | 145 | 3.0 | 0.0427 | 0.0236 | -0.0134 | 10.6 |
| Frances | 2004 | 25 Aug 00 UTC | 14.75 | 125 | 2.8 | 0.0523 | 0.0205 | -0.0090 | 4.2 |
| Ivan | 2004 | 02 Sep 18 UTC | 15.75 | 145 | 1.1 | 0.0355 | 0.0254 | -0.0100 | 10.4 |
| Katrina | 2005 | 23 Aug 18 UTC | 7.00 | 150 | 3.4 | 0.0494 | 0.0216 | 0.0065 | 7.6 |
| Wilma | 2005 | 15 Oct 18 UTC | 10.00 | 160 | 5.9 | 0.0633 | 0.0180 | -0.0051 | 10.5 |
| Epsilon | 2005 | 29 Nov 12 UTC | 9.25 | 75 | 2.4 | 0.0010 | 0.0012 | -0.0046 | 6.3 |
| Ernesto | 2006 | 24 Aug 18 UTC | 7.75 | 65 | 1.4 | 0.0628 | 0.0192 | -0.0062 | 8.1 |
| Helene | 2006 | 12 Sep 12 UTC | 12.00 | 105 | 3.6 | 0.0647 | 0.0115 | -0.0026 | 7.3 |
| Average | -- | -- | 11.50 | 108 | 3.1 | 0.0524 | 0.0143 | -0.0066 | 7.6 |

Table 2. The values of the constants in the LGE model when fitted to all forecast cases from 2001-2006 and the mean absolute error averaged over all storms and forecast times.

| Terms in $\kappa$ equation | $\beta$ ($hr^{-1}$) | n | b ($hr^{-1}$) | $a_1$ ($hr^{-1}$) | $a_2$($hr^{-1}$) | $a_3$($hr^{-1}$) | MAE (kt) |
|---|---|---|---|---|---|---|---|
| b | 0.0381 | 2.63 | .0113 | -- | -- | -- | 14.2 |
| b, C | 0.0261 | 2.71 | .0087 | -- | .0031 | -- | 13.4 |
| b, S | 0.0301 | 2.57 | .0077 | -.0088 | -- | -- | 11.7 |
| b, S, C | 0.0250 | 2.63 | .0066 | -.0077 | .0022 | -- | 11.3 |
| b, S, C, SC | 0.0253 | 2.60 | .0062 | -.0085 | .0005 | -.0041 | 11.0 |

**Figure Captions**

Figure 1. The analytic solution to the non-dimensional form of the logistic growth equation with positive $\kappa$ and n=3 for several values of the initial condition $U_o$.

Figure 2. Same as Fig. 1 but for negative $\kappa$.

Figure 3. The analytic solution to the non-dimensional form of the logistic growth equation with $U_o = 0.25$ for several values of n.

Figure 4. Scatter plot of the MPI estimated from the empirical formula of DeMaria and Kaplan and the theoretical formula of Bister and Emanuel for all Atlantic TCs from 1982-2006.

Figure 5. The 14.75 day LGEM forecast of the intensity of Hurricane Frances (2004) and the corresponding NHC best track intensity. The MPI estimated from the SST is also shown.

Figure 6. The 7 day LGEM forecast of the intensity of Hurricane Katrina (2005) and the corresponding NHC best track intensity. The MPI estimated from the SST is also shown.

Figure 7. The vertical velocity as a function of height from the entraining plume model. The temperature and moisture profiles of the parcel environment are from a mean Atlantic hurricane season sounding. Three versions of the model were run where both entrainment and condensate weight were neglected, entrainment was neglected, and both entrainment and condensate weight were included.

Figure 8. The MAE of the LGEM intensity prediction as a function of time when the model was fit to 2465 forecasts from the 2001-2006 Atlantic Hurricane Seasons. The error is shown for various combinations of predictors included in the estimate of the model growth rate parameter.

Figure 9. The growth rate $\kappa$ as a function of vertical shear (S) and convective instability parameter (C).

Figure 10. The MPI adjustment factor as a function of vertical shear (S) and convective instability parameter (C).

Figure 11. The time evolution of the vertical shear (S) and convective instability (C) for Hurricane Katrina (2005) from its initial formation to just before its Gulf coast landfall. The average S-C values for all rapidly intensifying TCs, storm with secondary eyewall formation, and annular hurricanes from the 2001-2006 sample are also shown.

Figure 12. The time evolution of the vertical shear (S) and convective instability (C) for Hurricane Claudette (2003) from its initial formation to just before its Texas coast landfall.

Figure 13. A conceptual diagram illustrating the use of the S-C phase space to anticipate tropical cyclone behavior.

Figure 14. The improvement of the real-time Atlantic and east Pacific LGEM intensity forecasts relative to the operational SHIPS forecasts for the combined 2006-2007 season samples.

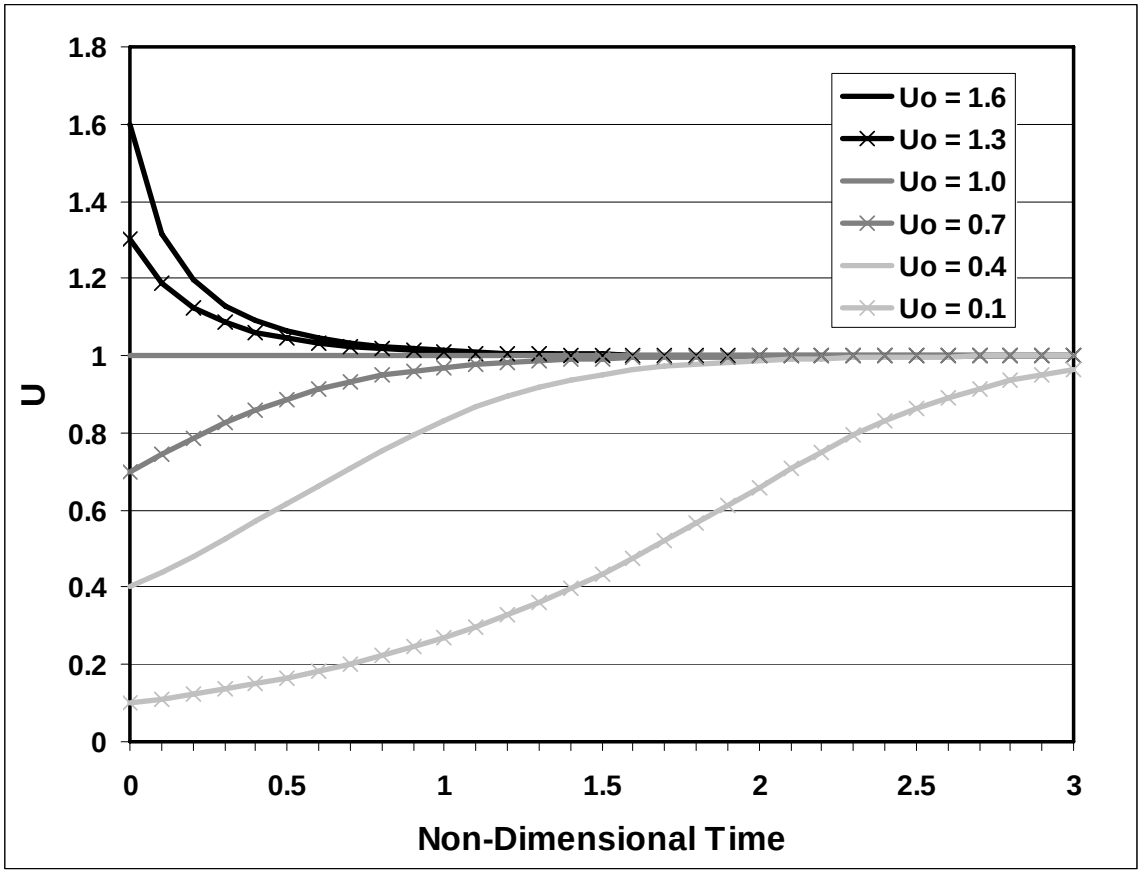


Figure 1. The analytic solution to the non-dimensional form of the logistic growth equation with positive $\kappa$ and n=3 for several values of the initial condition $U_o$.

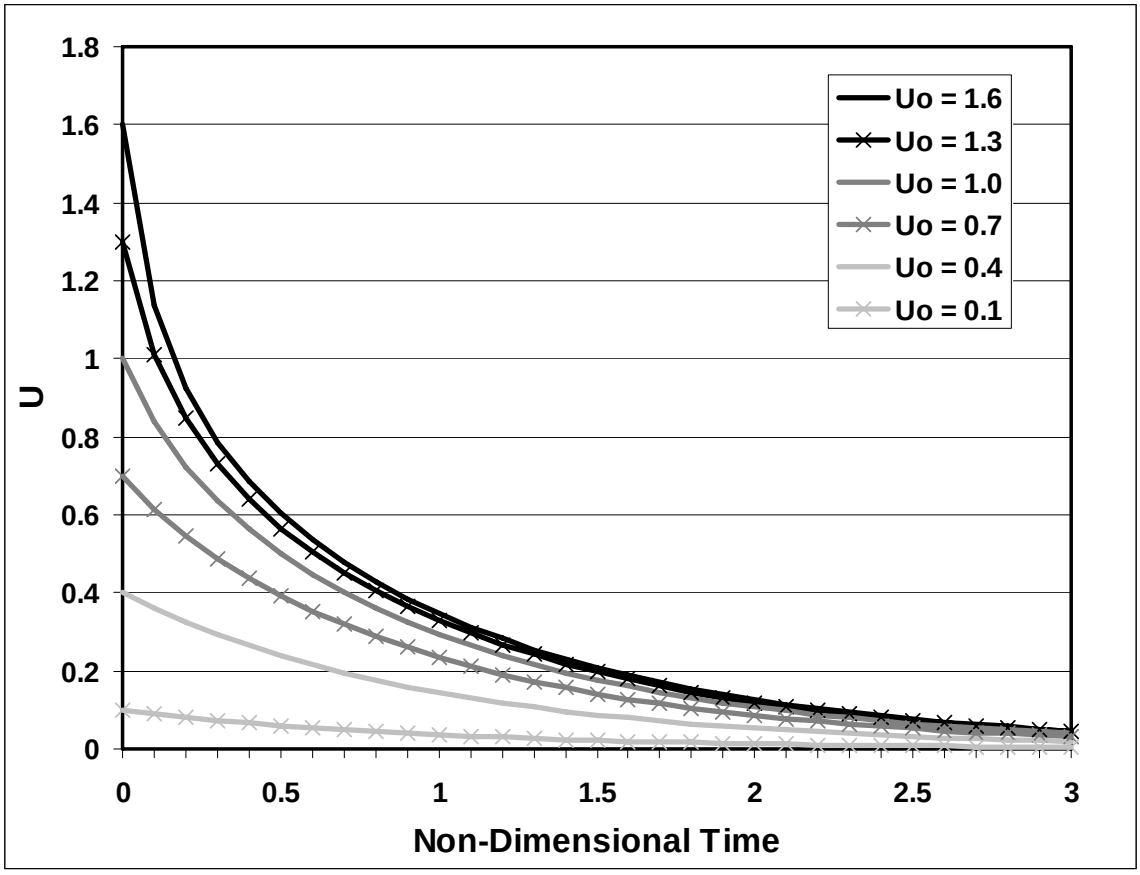


Figure 2. Same as Fig. 1 but for negative κ.

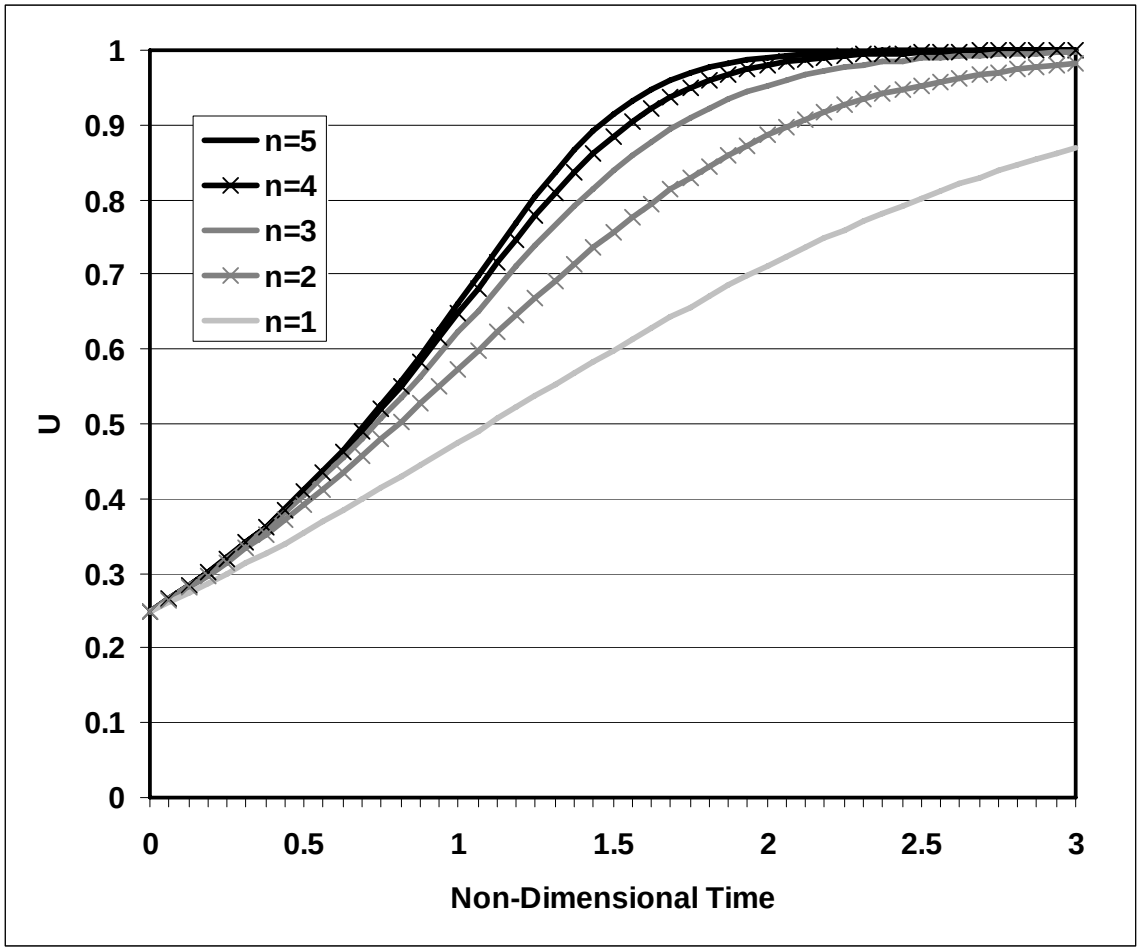


Figure 3. The analytic solution to the non-dimensional form of the logistic growth equation with $U_o = 0.25$ for several values of n.

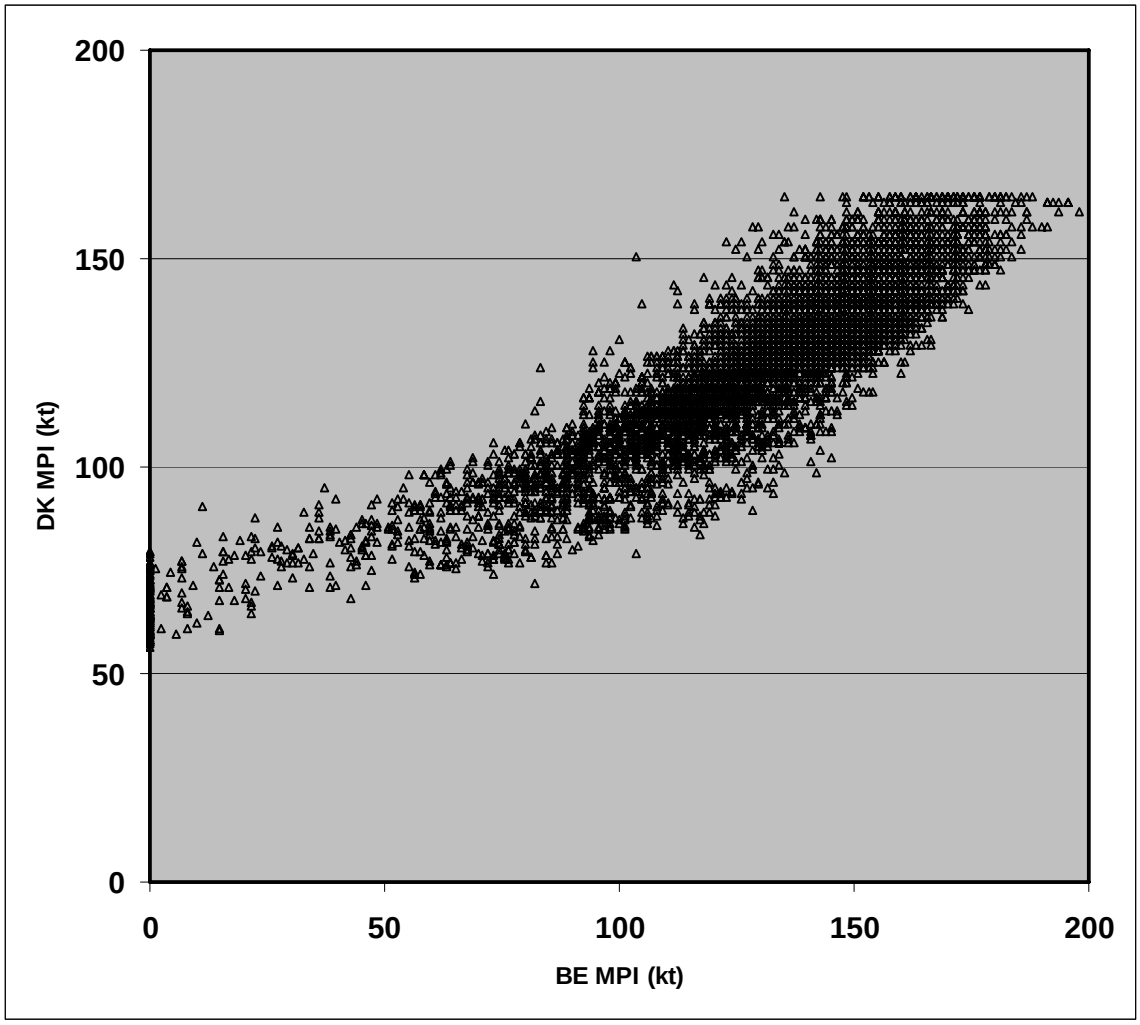


Figure 4. Scatter plot of the MPI estimated from the empirical formula of DeMaria and Kaplan and the theoretical formula of Bister and Emanuel for all Atlantic tropical cyclones from 1982-2006.

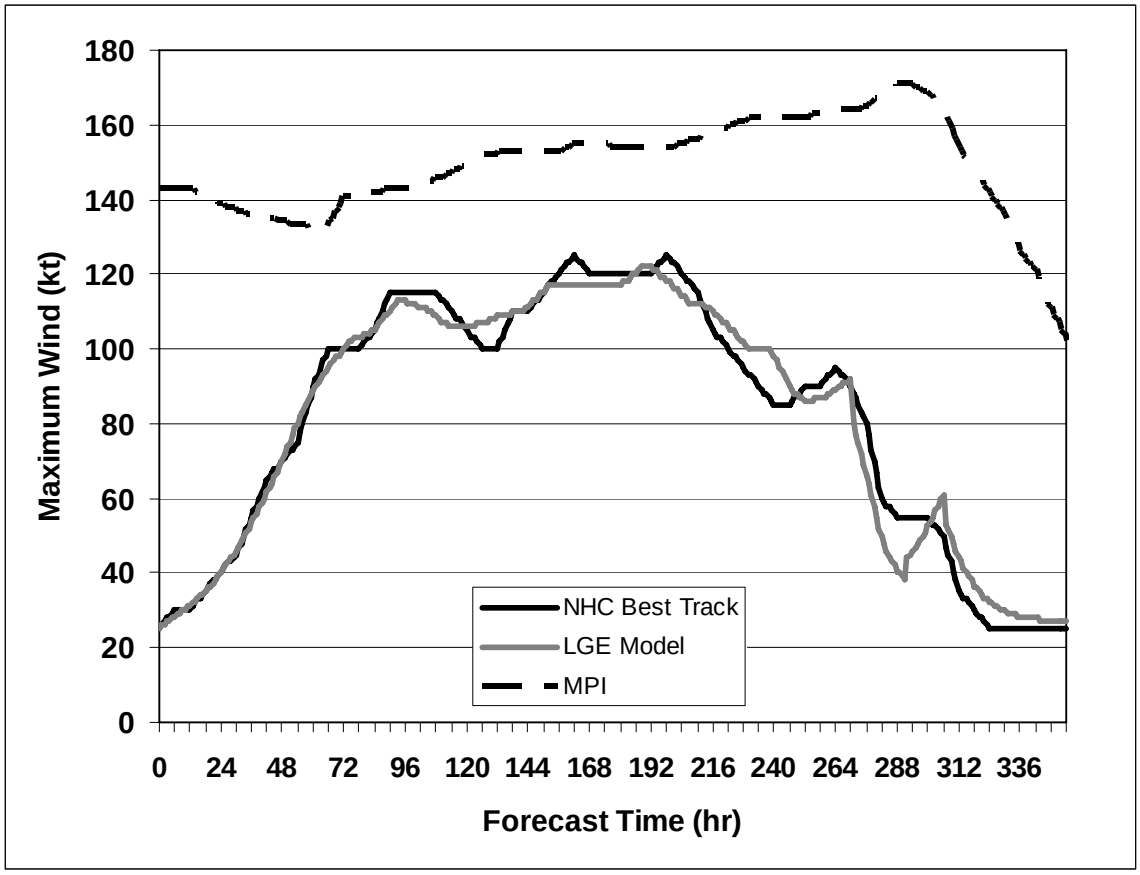


Figure 5. The 14.75 day LGEM forecast of the intensity of Hurricane Frances (2004) and the corresponding NHC best track intensity. The MPI estimated from the SST is also shown.

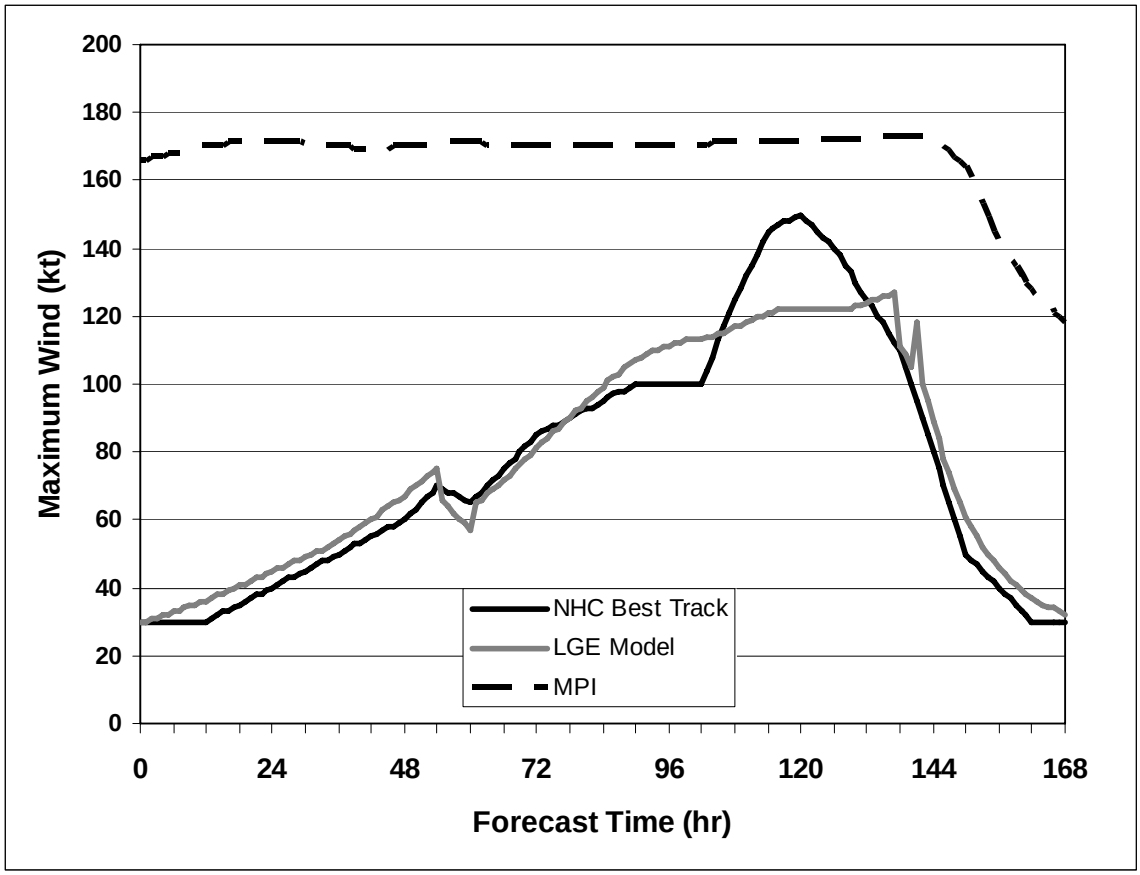


Figure 6. The 7 day LGEM forecast of the intensity of Hurricane Katrina (2005) and the corresponding NHC best track intensity. The MPI estimated from the SST is also shown.

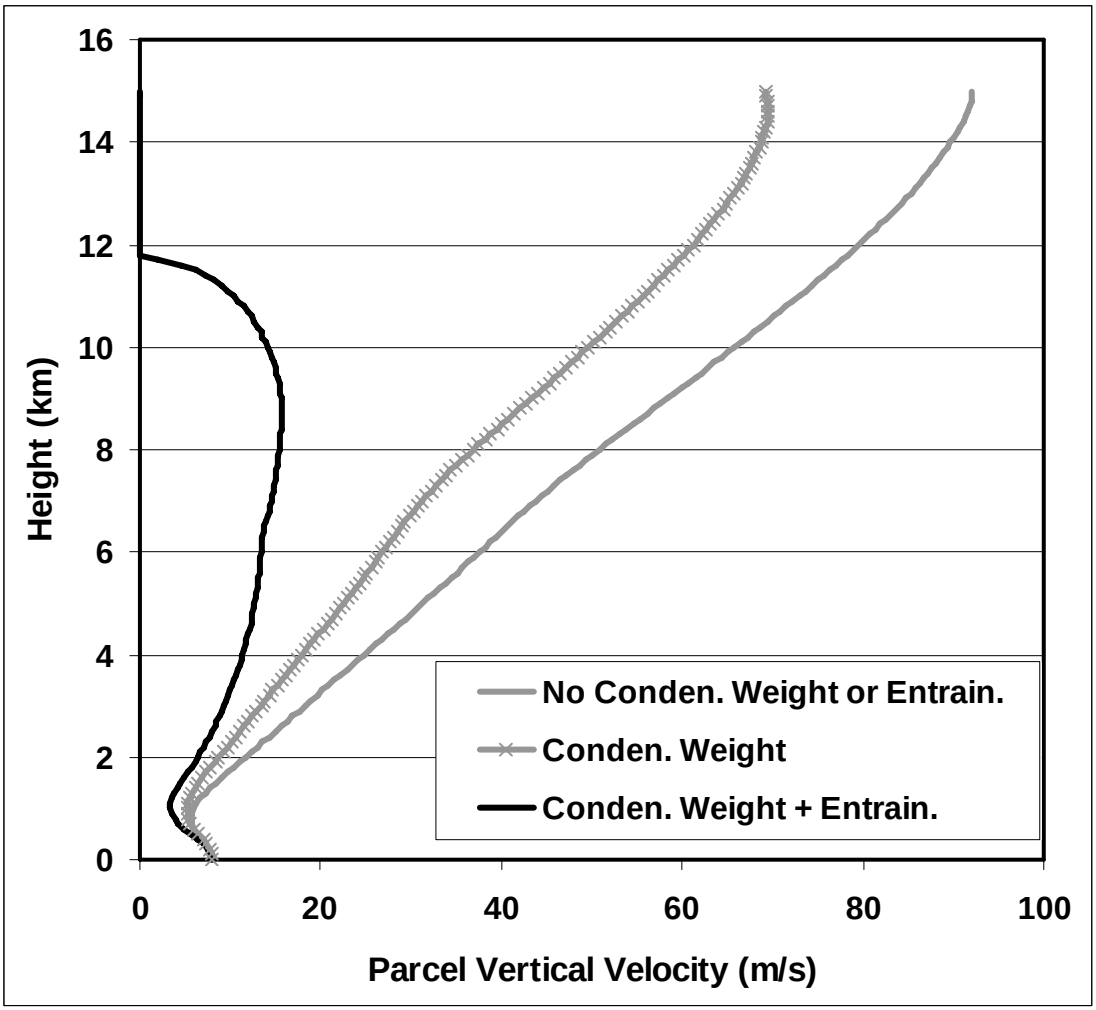


Figure 7. The vertical velocity as a function of height from the entraining plume model. The temperature and moisture profiles of the parcel environment are from a mean Atlantic hurricane sounding. Three versions of the model were run where both entrainment and condensate weight were neglected, entrainment was neglected, and both entrainment and condensate weight were included.

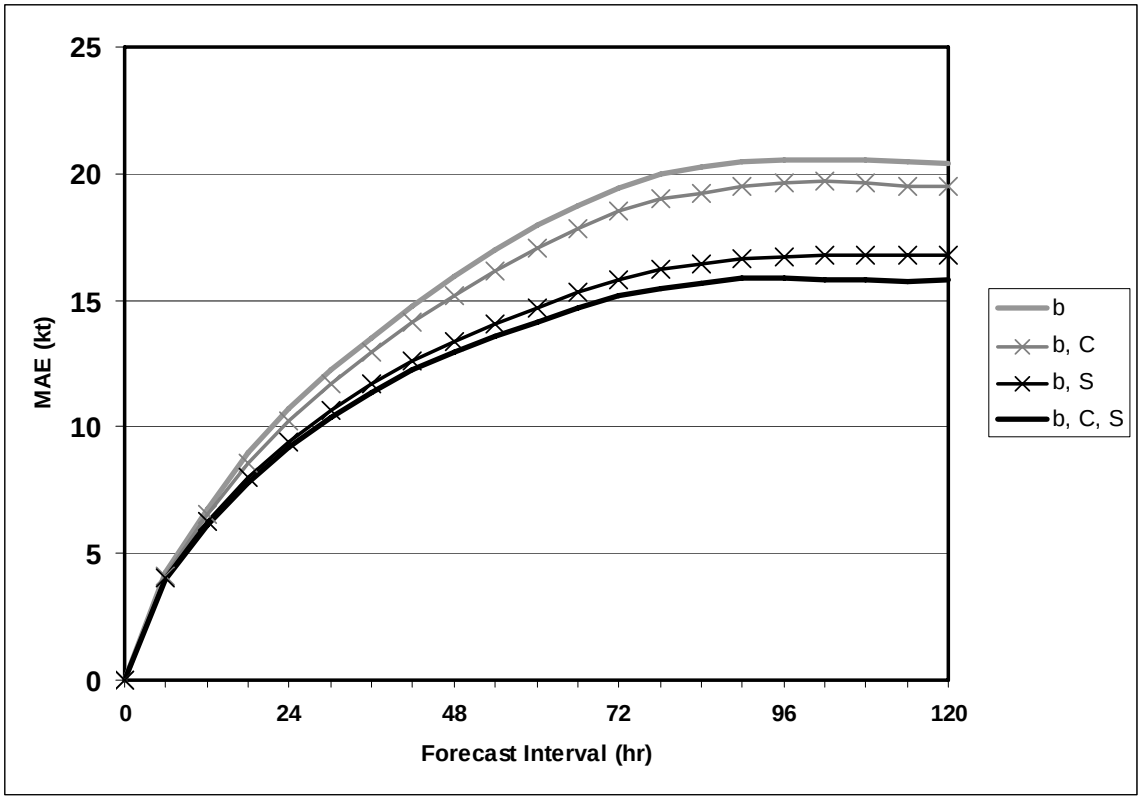


Figure 8. The MAE of the LGEM intensity prediction as a function of time when the model was fit to 2465 forecasts from the 2001-2006 Atlantic Hurricane Seasons. The error is shown for various combinations of predictors included in the estimate of the model growth rate parameter.

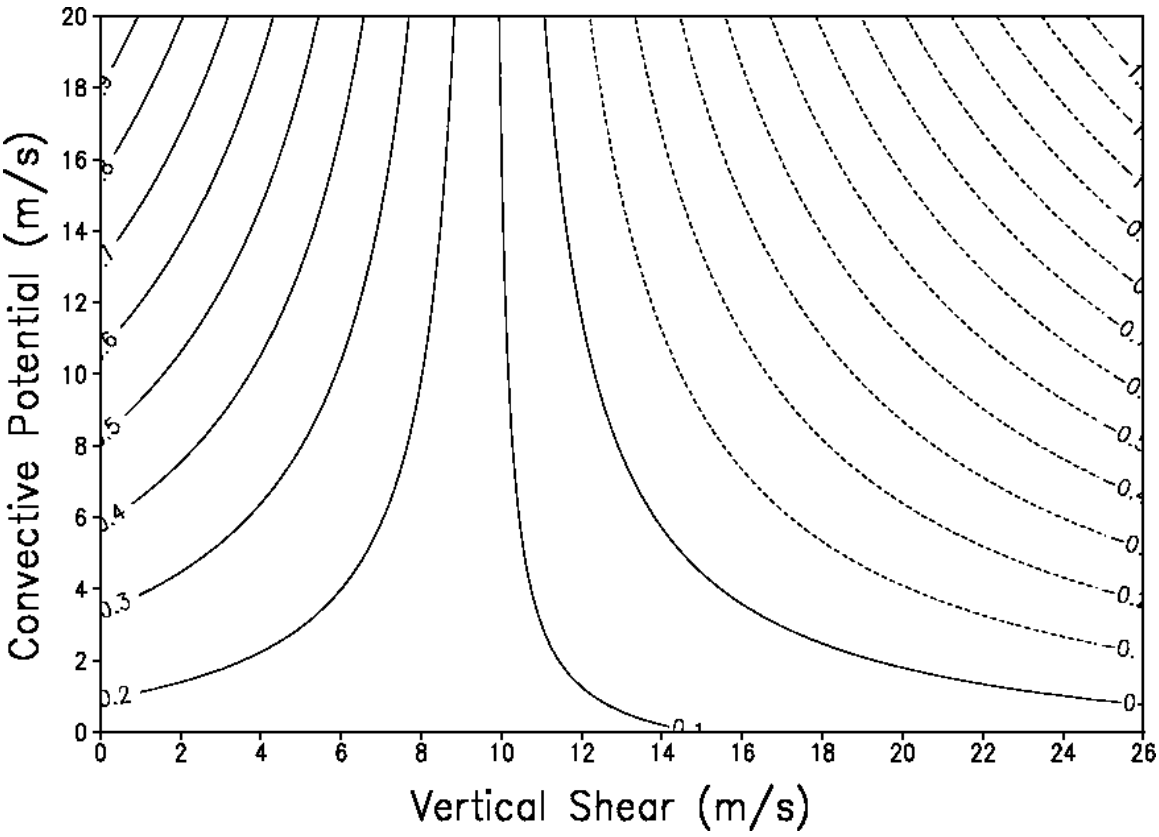


Figure 9. The growth rate κ as a function of vertical shear (S) and convective instability parameter (C).

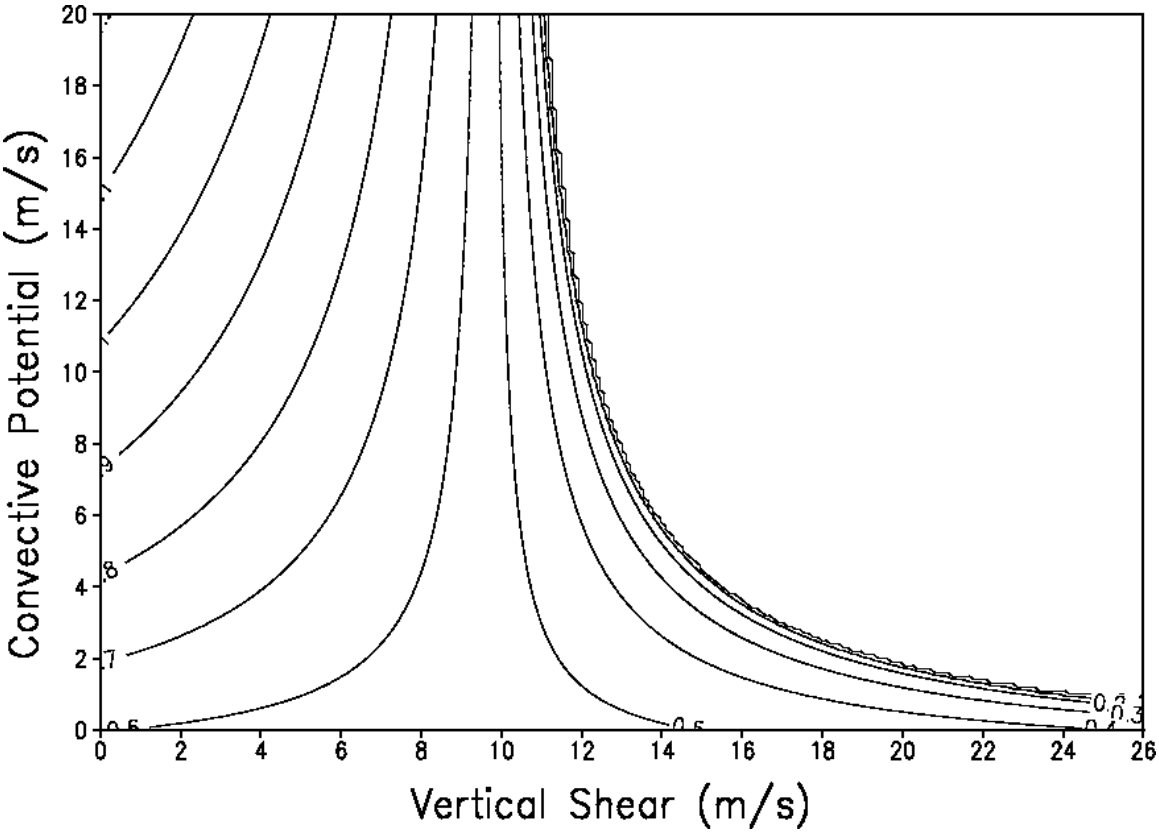


Figure 10. The MPI adjustment factor as a function of vertical shear (S) and convective instability parameter (C).

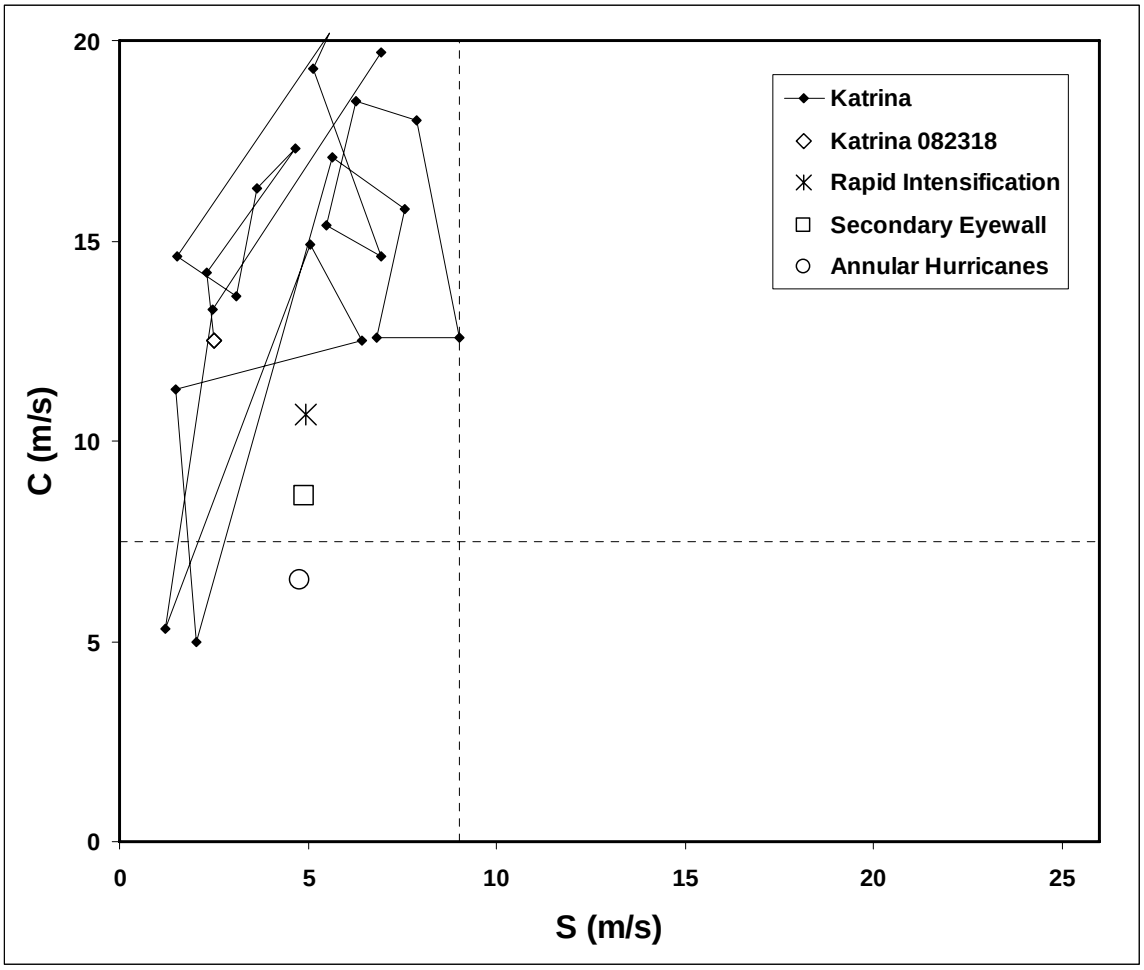


Figure 11. The time evolution of the vertical shear (S) and convective instability (C) for Hurricane Katrina (2005) from its initial formation to just before its Gulf coast landfall. The average S-C values for all rapidly intensifying TCs, storm with secondary eyewall formation, and annular hurricanes from the 2001-2006 sample are also shown.

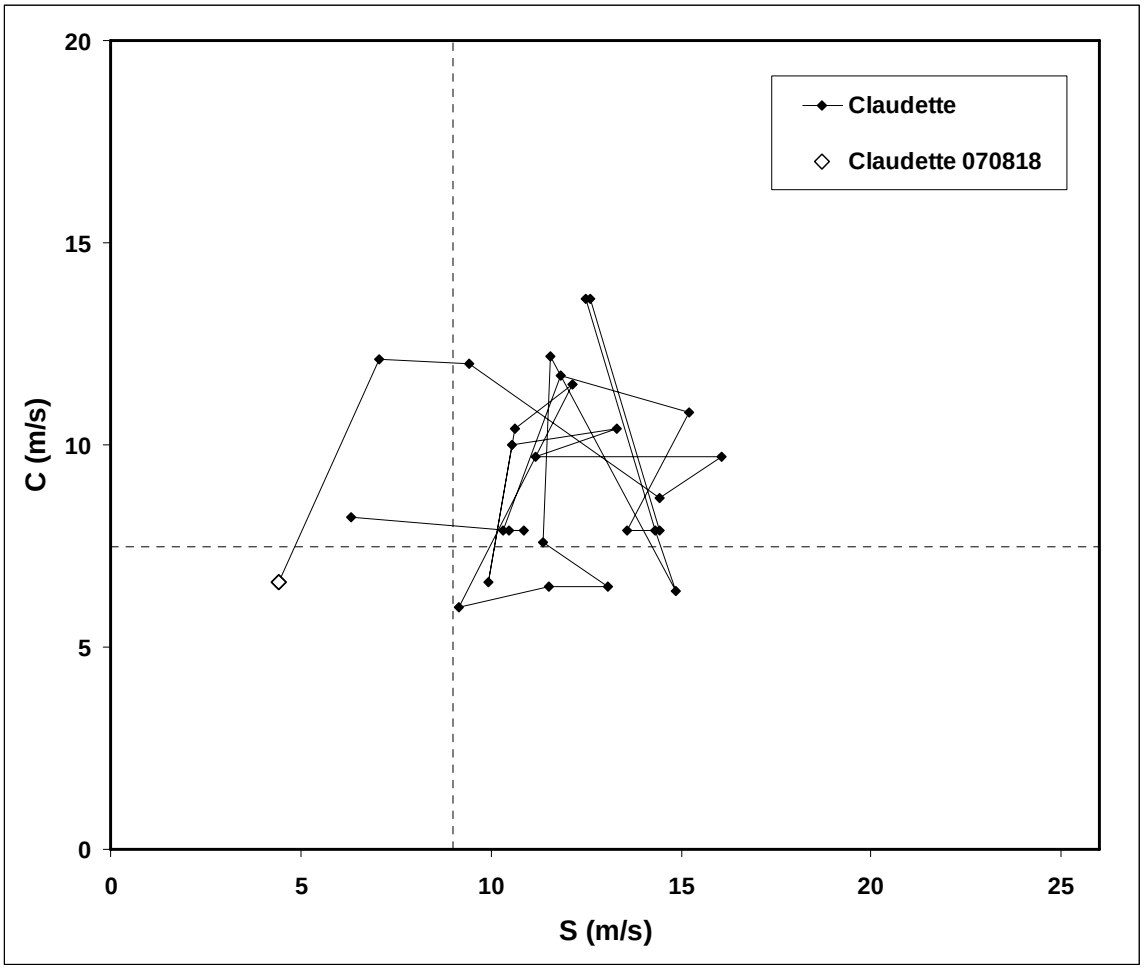


Figure 12. The time evolution of the vertical shear (S) and convective instability (C) for Hurricane Claudette (2003) from its initial formation to just before its Texas coast landfall.

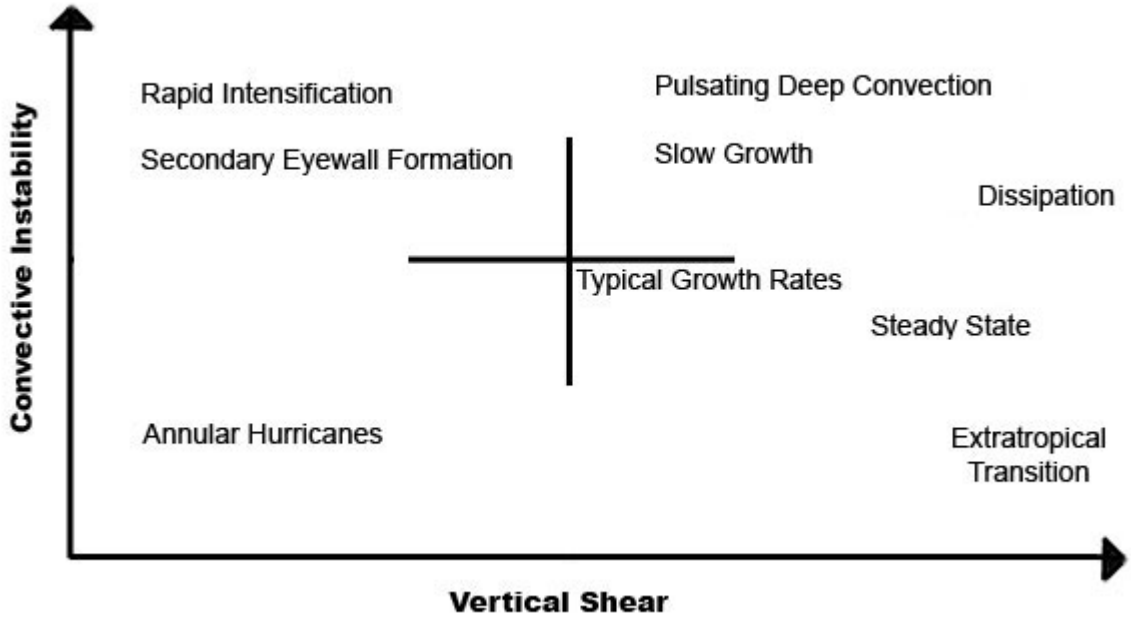


Figure 13. A conceptual diagram illustrating the use of the S-C phase space to anticipate tropical cyclone behavior.

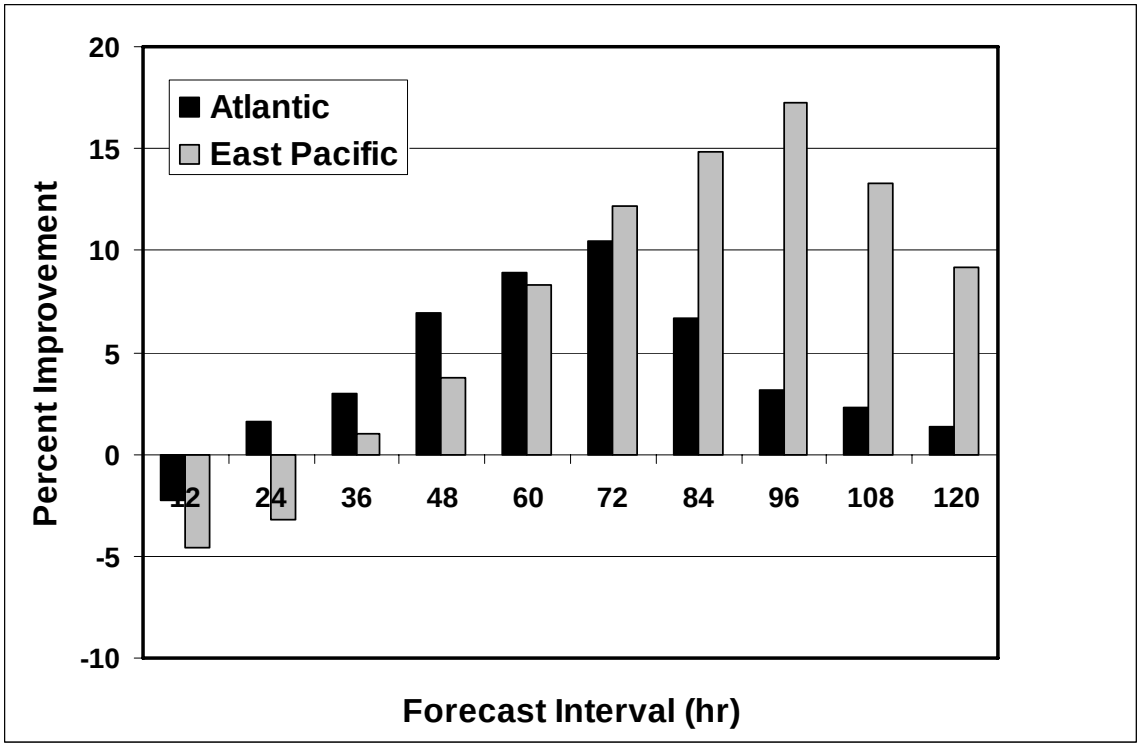


Figure 14. The improvement of the real-time Atlantic and east Pacific LGEM intensity forecasts relative to the operational SHIPS forecasts for the combined 2006-2007 season samples.